5 Transfer-Matrix Approach to Classical Systems

T. Nishino[1], K. Okunishi[2], Y. Hieida[2], T. Hikihara[1], and H. Takasaki[1]

[1] Department of Physics, Graduate School of Science and Technology, Kobe University, Inoshishi-dai, Nada, Kobe 657-8501, Japan
[2] Department of Physics, Graduate School of Science, Osaka University, Toyonaka, Osaka 560-0043, Japan

The development of the DMRG method by White [1] is one of the major achievements in computational condensed matter physics (see Chap. 2(I)). DMRG enables one to calculate ground states of relatively large scale one-dimensional (1D) quantum systems. Since 1D quantum systems are deeply related to 2D classical systems [2–4], it is natural to import the DMRG method to 2D classical systems. The infinite-system algorithm was first applied to the Ising model by one of the authors [5]. Carlon *et al.* [6–8] applied the finite system algorithm to the Potts model (Chap. 3.2(II)), and they calculated very accurate density profiles and critical indices. After that, the DMRG formulation for classical systems was applied to 1D quantum system at finite temperature [9,10,12] (Chaps. 6(I) and 4(II)).

In this review we explain the DMRG applied to 2D classical systems ('classical DMRG') by looking at the renormalization group (RG) transformation for the transfer matrix T. For the distinction, we call the DMRG for quantum systems 'quantum DMRG' in the following. We first introduce the infinite-system algorithm (Sects.1-4). It then follows naturally that the classical DMRG is a kind of variational method that maximizes the partition function using a limited number of degrees of freedom, where the variational state is written as a product of local matrices [15] (Sect.5). Actually, such a variational formulation has been used for a long time; we give a brief review in Sect.6. The variational state obtained by the infinite-system algorithm can be improved systematically by use of the finite-system algorithm (Sect.7). As a variation of the infinite system algorithm, we introduce the corner transfer matrix (CTM) formulation of the classical DMRG, where the formulation can be generalized to higher-dimensional systems (Sect.8). We finally discuss some remaining problems in the last section.

1 Transfer Matrix

As an example of a 2D classical system, let us consider the isotropic square-lattice Ising model [17] on a cylinder, which is defined by imposing periodic boundary conditions in the vertical direction and open boundary conditions for the horizontal direction of an $(N \times \ell)$ spin lattice (Fig.1) [16]. The system

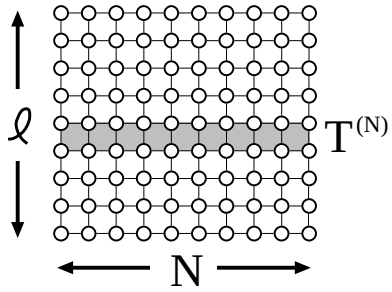

Fig. 1. Square lattice Ising model on a N by ℓ rectangular lattice constructed by stacking ℓ transfer matrices $T^{(N)}$ defined in (1). Open boundary conditions are imposed in the horizontal direction and periodic ones in the vertical direction.

consists of ℓ rows of width N. We assume $\ell \gg N$, and refer to N as the system size. We label the spins in a row from left to right as $s_1, s_2, \ldots, s_{N-1}, s_N$, and occasionally use the vector notation $\boldsymbol{s} = s_{1\ldots}s_N$ for simplicitely. When the Ising interaction is restricted to the nearest neighbor pairs, the transfer matrix is expressed as a 2^N-dimensional matrix (Fig.2)

$$T^{(N)}(\boldsymbol{s}'|\boldsymbol{s}) = \exp\left\{\frac{K}{2}\sum_{i=1}^{N-1}(s'_i s'_{i+1} + s_i s_{i+1}) + K\sum_{i=1}^{N} s'_i s_i\right\} \tag{1}$$

$$= \exp\left(\frac{K}{2}s_1 s'_1\right)\left\{\prod_{i=1}^{N-1} W(s'_i s'_{i+1}|s_i s_{i+1})\right\}\exp\left(\frac{K}{2}s_N s'_N\right),$$

where $K = J/k_{\mathrm{B}}T$ is the coupling and

$$W(s'_i s'_{i+1}|s_i s_{i+1}) = \exp\left\{\frac{K}{2}\left(s_i s_{i+1} + s_{i+1}s'_{i+1} + s'_{i+1}s'_i + s'_i s_i\right)\right\} \tag{2}$$

is the local Boltzmann weight for a square between i and $i+1$. We have symmetrized the transfer matrix in order to simplify the following formulation. It may be helpful for the readers to recall the quantum-classical correspondence $T^{(N)} = \exp(-\Delta H^{(N)})$, where $H^{(N)}$ is the corresponding quantum Hamiltonian. (However, $H^{(N)}$ is normally non-local and the correspondence is more of a formal character.)

For a tutorial purpose, we only consider the symmetric transfer matrix in the following. Extensions to the asymmetric case are straightforward [5,18]; to treat an asymmetric transfer matrix is not rare in classical statistical mechanics. The details are explained by Xiang and Wang in Chaps. 6(I), 4.1(II) [10,11] as well as by Shibata in Chap. 4.2(II) [12,13]. More generally, it is possible to treat various models such as

- The q-state Potts model [19,20] or the n-vector model, that have *discrete spin symmetry and short range interaction.*

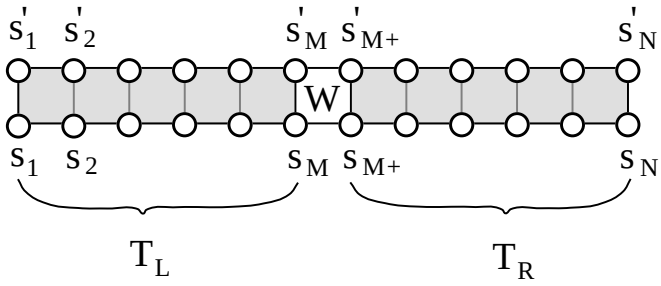

Fig. 2. Division of the transfer matrix $T^{(N)}$ into the half-row transfer matrices T_L and T_R, and a Boltzmann weight W, compare (3).

- The interaction round a face (IRF) model [18] whose Boltzmann weight $W(s'_i s'_{i+1}|s_i s_{i+1})$ is represented by arbitrary matrix; *the weight can even be negative.* [14] (There is no sign problem.)
- The vertex model [18] that has spin variables in the middle of each bond.

in the framework of DMRG.

Following the convention of the quantum DMRG, let us divide the spin row into the left and the right as $\boldsymbol{s} = \boldsymbol{s}_L \boldsymbol{s}_R$, where $\boldsymbol{s}_L = s_{1\ldots}s_M$ and $\boldsymbol{s}_R = s_{M+1\ldots}s_N$. For the moment we assume that N is an even integer, and that $M = N/2$. According to the division, we can decompose $T^{(N)}$ into three factors

$$T^{(N)}(\boldsymbol{s}'|\boldsymbol{s}) = T_L(\boldsymbol{s}'_L|\boldsymbol{s}_L) W(s'_M s'_{M+1}|s_M s_{M+1}) T_R(\boldsymbol{s}'_R|\boldsymbol{s}_R)\,, \tag{3}$$

where $T_L(\boldsymbol{s}'_L|\boldsymbol{s}_L)$ and $T_R(\boldsymbol{s}'_R|\boldsymbol{s}_R)$ are the half-row transfer matrices

$$\begin{aligned} T_L(\boldsymbol{s}'_L|\boldsymbol{s}_L) &= \exp\left(\frac{K}{2}\, s'_1 s_1\right) \prod_{i=1}^{M-1} W(s'_i s'_{i+1}|s_i s_{i+1}) \\ T_R(\boldsymbol{s}'_R|\boldsymbol{s}_R) &= \exp\left(\frac{K}{2} s'_N s_N\right) \prod_{i=M+1}^{N-1} W(s'_i s'_{i+1}|s_i s_{i+1})\,. \end{aligned} \tag{4}$$

2 Density Submatrix

The density matrix of the N by ℓ system (Fig.1) is simply the ℓ-th power of the transfer matrix $\rho = (T^{(N)})^\ell$. The partition function is its trace

$$Z = \operatorname{Tr}\rho = \operatorname{Tr}(T^{(N)})^\ell = \sum_\kappa \lambda_\kappa{}^\ell\,, \tag{5}$$

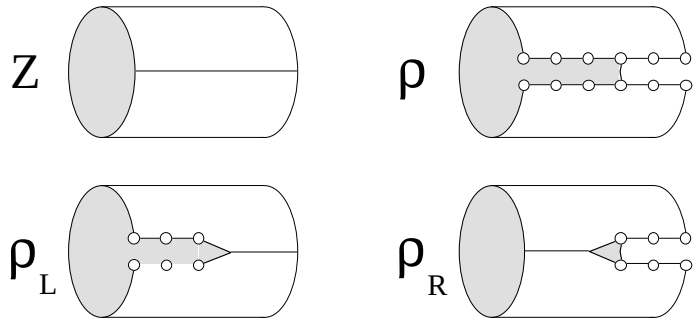

Fig. 3. Graphical representation for ρ, Z (5), ρ_L and ρ_R (7). The DSM can be interpreted as a cut in the 2D system shown in Fig.1.

where λ_κ is the eigenvalue of $T^{(N)}$ in the decreasing order $\lambda_1 \geq \lambda_2 \geq \cdots \geq 0$. (We have assumed that the transfer matrix is diagonalizable, and that all the eigenvalues are positive.) Since we have assumed that ℓ is sufficiently larger than N, the partition function can be approximated as $Z \simeq {\lambda_1}^\ell$, where the symbol '$\simeq$' denotes that the ratio ${\lambda_1}^\ell/Z$ converges to unity in the limit $\ell/N \to \infty$. In this situation, the density matrix can be well approximated as

$$\rho \simeq |v^{(N)}\rangle \, {\lambda_1}^\ell \, \langle v^{(N)}| \tag{6}$$

where $|v^{(N)}\rangle$ is the eigenvector of $T^{(N)}$ that corresponds to the largest eigenvalue λ_1. We assume the normalization $\langle v^{(N)}|v^{(N)}\rangle = 1$.

What is called 'density matrix' in the context of DMRG is not the density matrix itself, but the density submatrix (DSM) — also called 'reduced density matrix' — which is obtained by partially tracing out spin indices from ρ. The DSM for the left and the right halves of the system are defined as [21]

$$\begin{aligned} \rho_L(\boldsymbol{s}'_L|\boldsymbol{s}_L) &= \sum_{\boldsymbol{s}_R} \rho(\boldsymbol{s}'_L\, \boldsymbol{s}_R|\boldsymbol{s}_L\, \boldsymbol{s}_R) \\ \rho_R(\boldsymbol{s}'_R|\boldsymbol{s}_R) &= \sum_{\boldsymbol{s}_L} \rho(\boldsymbol{s}_L\, \boldsymbol{s}'_R|\boldsymbol{s}_L\, \boldsymbol{s}_R)\,. \end{aligned} \tag{7}$$

Figure 3 shows the graphical representation of the DSM, where ρ_L and ρ_R correspond to the cuts on the cylindrical system shown in Fig.1 [22]. To take the trace of the DSM one has to join the system along the cut and to reconstruct the cylinder: $Z = \mathrm{Tr}\,\rho_L = \mathrm{Tr}\,\rho_R$. Using the eigenvector $v^{(N)}$ in

(6), we can express the DSM in the more familiar form

$$\rho_L(\boldsymbol{s}'_L|\boldsymbol{s}_L) \simeq \sum_{\boldsymbol{s}_R} v^{(N)}(\boldsymbol{s}'_L\, \boldsymbol{s}_R)\, {\lambda_1}^{\ell}\, v^{(N)}(\boldsymbol{s}_L\, \boldsymbol{s}_R)$$
$$\rho_R(\boldsymbol{s}'_R|\boldsymbol{s}_R) \simeq \sum_{\boldsymbol{s}_L} v^{(N)}(\boldsymbol{s}_L\, \boldsymbol{s}'_R)\, {\lambda_1}^{\ell}\, v^{(N)}(\boldsymbol{s}_L\, \boldsymbol{s}_R) \tag{8}$$

that has been used for the quantum DMRG.

As for the quantum DMRG, the diagonalization of the DSM is one of the important steps for the classical DMRG. The DSM ρ_L and ρ_R can be diagonalized as

$$\rho_L = \sum_{\xi} \boldsymbol{a}_\xi\, {\omega_\xi}^2\, {\boldsymbol{a}_\xi}^T\,, \qquad \rho_R = \sum_{\zeta} \boldsymbol{b}_\zeta\, {\mu_\zeta}^2\, {\boldsymbol{b}_\zeta}^T\,, \tag{9}$$

where $\boldsymbol{a}_\xi$ and $\boldsymbol{b}_\xi$ are the eigenvectors of ρ_L and ρ_R, respectively. The eigenvectors satisfy the orthogonality relations ${\boldsymbol{a}_\xi}^T \boldsymbol{a}_{\xi'} = \delta_{\xi\xi'}$ and ${\boldsymbol{b}_\zeta}^T \boldsymbol{b}_{\zeta'} = \delta_{\zeta\zeta'}$, and they are complete

$$I_L = \sum_{\xi} \boldsymbol{a}_\xi\, {\boldsymbol{a}_\xi}^T\,, \qquad I_R = \sum_{\zeta} \boldsymbol{b}_\zeta\, {\boldsymbol{b}_\zeta}^T\,, \tag{10}$$

where I_L and I_R are 2^M- and 2^{N-M}-dimensional unit matrices, respectively; $I_L = I_R$ when $N = 2M$. It is convenient to use the matrix notation $A = (\boldsymbol{a}_1, \boldsymbol{a}_2, \cdots)$ and $B = (\boldsymbol{b}_1, \boldsymbol{b}_2, \cdots)$ when we explicitly show the spin indices. For example, (9) can be written as

$$\rho_L(\boldsymbol{s}'_L|\boldsymbol{s}_L) = \sum_{\xi} A(\boldsymbol{s}'_L|\xi)\, {\omega_\xi}^2\, A(\boldsymbol{s}_L|\xi)$$
$$\rho_R(\boldsymbol{s}'_R|\boldsymbol{s}_R) = \sum_{\zeta} B(\boldsymbol{s}'_R|\zeta)\, {\mu_\zeta}^2\, B(\boldsymbol{s}_R|\zeta)\,. \tag{11}$$

In (9) and (11) we have expressed the eigenvalues of ρ_L and ρ_R as squares of real numbers, because normally they are non-negative [23]. As to the eigenvalues of ρ, we assume decreasing order for both ${\omega_\xi}^2$ and ${\mu_\zeta}^2$

$${\omega_1}^2 \geq {\omega_2}^2 \geq \cdots \geq 0\,, \qquad {\mu_1}^2 \geq {\mu_2}^2 \geq \cdots \geq 0\,, \tag{12}$$

in the following. In general, $\omega_i = \mu_i$ holds for $1 \leq i \leq \min(2^M, 2^{N-M})$ in the limit $\ell/N \to \infty$.

3 Renormalization Group Transformation

Unlike the density matrix ρ, not only the largest eigenvalue is dominant in (12). This is because $\boldsymbol{s}'_L$ and $\boldsymbol{s}_L$ in $\rho_L(\boldsymbol{s}'_L|\boldsymbol{s}_L)$ are correlated through the

junction $\boldsymbol{s}_R$ (7)-(8). It has been known that the eigenvalues ${\omega_i}^2$ (or ${\mu_i}^2$) in (12) decay nearly exponentially when the correlation length of the system is finite [18,24,25] (Chap. 3.1(II)), and that the decay is rapid when the correlation length is short. Even at the critical temperature, we expect a certain decay in ${\omega_i}^2$, because the system size N is finite and the correlation length is of the order of N. As a result we can say that the partition function can be approximated by the partial sum of the DSM eigenvalues

$$\tilde{Z} = \sum_{i=1}^{m} {\omega_i}^2 \,, \tag{13}$$

where m is the number of the eigenvalues kept. It is obvious that $Z \geq \tilde{Z}$, and the difference $Z - \tilde{Z}$ is fairly small when m is sufficiently large. We can also express $\tilde{Z}$ as

$$\tilde{Z} = \mathrm{Tr}\,(P_L\,\rho_L) = \mathrm{Tr}\,\tilde{\rho}_L \tag{14}$$

where P_L is a projection operator

$$P_L(\boldsymbol{s}'_L|\boldsymbol{s}_L) = \sum_{\xi=1}^{m} A(\boldsymbol{s}'_L|\xi)A(\boldsymbol{s}_L|\xi)\,, \tag{15}$$

and therefore $\tilde{\rho}_L$ is an m-dimensional diagonal matrix

$$\tilde{\rho}_L(\xi'|\xi) = \sum_{\boldsymbol{s}'_L \boldsymbol{s}_L} A(\boldsymbol{s}'_L|\xi')\rho_L(\boldsymbol{s}'_L|\boldsymbol{s}_L)A(\boldsymbol{s}_L|\xi) \;=\; \delta_{\xi'\,\xi}\,\omega_\xi^2 \tag{16}$$

where $\xi', \xi \leq m$. (If $m = 2^M$, P_L coincides with I_L in (10).) From (14)-(16), the transformation $\rho_L \to \tilde{\rho}_L$ by $A(\boldsymbol{s}_L|\xi)$ in (16) can be regarded as the RG transformation from the row spin $\boldsymbol{s}_L$ to an m-state block spin ξ. In the same manner $B(\boldsymbol{s}_R|\zeta)$ is related to the RG transformation $\boldsymbol{s}_R \to \zeta$, that performs the mapping $\rho_R \to \tilde{\rho}_R$. In the following, we put a tilde over the renormalized matrices.

It should be noted that the RG transformation $\rho_L \to \tilde{\rho}_L$ is performed so that it maximizes the approximate partition function $\tilde{Z}$ within the restricted number of degrees of freedom m. On the other hand, the RG transformation in quantum DMRG minimizes the ground state energy; this is consistent with the thermodynamic relation $F = -k_{\mathrm{B}}T \log Z = U - TS$ in the limit $T \to 0$.

4 Infinite-System Algorithm

In quantum DMRG, the infinite-system algorithm consists of the iterative use of the system expansion and the RG transformation for the Hamiltonian. It is easy to introduce the RG process to 2D classical system, using the quantum-classical correspondence $T^{(N)} = \exp(-\Delta H^{(N)})$; as far as the formulation is

concerned, the classical DMRG can be obtained just by replacing the Hamiltonian $H^{(N)}$ in quantum DMRG by the transfer matrix $T^{(N)}$. As we show in this section, the infinite-system algorithm constructs renormalized transfer matrices $\tilde{T}^{(6)}, \tilde{T}^{(8)}, \ldots, \tilde{T}^{(N)}$ successively up to arbitrary N.

The infinite-system algorithm starts from the 4-site system, whose transfer matrix is given by

$$T^{(4)}(s_1' s_2' s_3' s_4' | s_1 s_2 s_3 s_4) = T_L(s_1' s_2' | s_1 s_2) W(s_2' s_3' | s_2 s_3) T_R(s_3' s_4' | s_3 s_4)\,. \quad (17)$$

Diagonalizing $T^{(4)}$, we obtain the largest eigenvalue and the corresponding eigenvector $v^{(4)}(s_1 s_2 s_3 s_4)$, that satisfies $T^{(4)} v^{(4)} = \lambda\, v^{(4)}$. We then obtain $\rho_L(s_1' s_2' | s_1 s_2)$ and $\rho_R(s_3' s_4' | s_3 s_4)$ using (8) and get the RG transformation matrices $A(s_1 s_2 | \xi)$ and $B(s_3 s_4 | \zeta)$ from the diagonalization of ρ_L and ρ_R (11).

The next step is the enlargement of the system from $N = 4$ to $N = 6$ and the RG transformation via the substitution

$$\sum_{s_1' s_2' s_1 s_2} A(s_1' s_2' | \xi') T_L(s_1' s_2' | s_1 s_2) W(s_2' s_3' | s_2 s_3) A(s_1 s_2 | \xi) \to \tilde{T}_L(\xi' s_3' | \xi s_3)$$

$$\sum_{s_5' s_6' s_5 s_6} B(s_5' s_6' | \zeta') W(s_4' s_5' | s_4 s_5) T_R(s_5' s_6' | s_5 s_6) B(s_5 s_6 | \zeta) \to \tilde{T}_R(s_4' \zeta' | s_4 \zeta)\,, \quad (18)$$

where $\tilde{T}_L$ and $\tilde{T}_R$ are the renormalized half-row transfer matrices. (We have changed the spin indices of T_R according to the enlargement $N = 4$ to $N = 6$.) The greek indices ξ and ζ represent the block variables, that take (at most) m values. This is shown graphically in Fig. 4. Joining $\tilde{T}_L$ and $\tilde{T}_R$, we can construct the renormalized transfer matrix for $N = 6$

$$\tilde{T}^{(6)}(\xi' s_3' s_4' \zeta' | \xi s_3 s_4 \zeta) = \tilde{T}_L(\xi' s_3' | \xi s_3) W(s_3' s_4' | s_3 s_4) \tilde{T}_R(s_4' \zeta' | s_4 \zeta)\,. \quad (19)$$

At this stage, ξ and ζ represent the 2-spin blocks.

It is obvious that we can obtain $\tilde{T}^{(8)}$ in the same manner, i.e., diagonalizing $\tilde{T}^{(6)}$ in (19) to obtain the largest eigenvalue and the corresponding eigenvector $\tilde{v}^{(6)}(\xi s_3 s_4 \zeta)$, and create $\tilde{\rho}_L(\xi' s_3' | \xi s_3)$ and to $\tilde{\rho}_R(s_4' \zeta' | s_4 \zeta)$, using an extension of (8). We obtain the RG transformations $A(\xi s_3 | \xi_{\rm new})$ and $B(s_4 \zeta | \zeta_{\rm new})$ by diagonalizing $\tilde{\rho}_L$ and $\tilde{\rho}_R$, (an extension of (11)) respectively, where $\xi_{\rm new}$ and $\zeta_{\rm new}$ are m-state variables that represent the 3-spin block. The $\tilde{T}^{(8)}$ is then constructed as

$$\begin{aligned}\tilde{T}^{(8)}&(\xi'_{\rm new} s_4' s_5' \zeta'_{\rm new} | \xi_{\rm new} s_4 s_5 \zeta_{\rm new}) \\ &= \tilde{T}_L(\xi'_{\rm new} s_4' | \xi_{\rm new} s_4) W(s_4' s_5' | s_4 s_5) \tilde{T}_R(s_5' \zeta'_{\rm new} | s_5 \zeta_{\rm new})\,, \end{aligned} \quad (20)$$

where $\tilde{T}_L(\xi'_{\rm new} s_4' | \xi_{\rm new} s_4)$ and $\tilde{T}_R(s_5' \zeta'_{\rm new} | s_5 \zeta_{\rm new})$ are created as

$$\sum_{\xi' s_3' \xi s_3} A(\xi' s_3' | \xi'_{\rm new}) \tilde{T}_L(\xi' s_3' | \xi s_3) W(s_3' s_4' | s_3 s_4) A(\xi s_3 | \xi_{\rm new}) \to \tilde{T}_L(\xi'_{\rm new} s_4' | \xi_{\rm new} s_4)$$

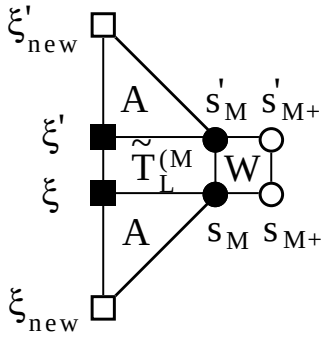

Fig. 4. Enlargement by W and RG transformation through A of the half-row transfer matrix $\tilde{T}_L$ in (18)-(21). The filled circles and squares denote variables which are summed.

$$\sum_{s_6'\zeta' s_6\zeta} B(s_6'\zeta'|\zeta'_{\rm new}) W(s_5's_6'|s_5s_6) \tilde{T}_R(s_6'\zeta'|s_6\zeta) B(s_6\zeta|\zeta_{\rm new}) \to \tilde{T}_R(s_5'\zeta'_{\rm new}|s_5\zeta_{\rm new})\,. \tag{21}$$

In this way, we further obtain $\tilde{T}^{(10)}$, $\tilde{T}^{(12)}$, $\tilde{T}^{(14)}$, ..., etc., up to arbitrary system size. This is the outline of the infinite-system algorithm.

Numerical diagonalization for $\tilde{T}^{(N)}$ is normally performed via the Lanczos method [26], that requires multiplication of $\tilde{T}^{(N)}$ with a $4m^2$-dimensional vector $\boldsymbol{x}$. Since $\tilde{T}^{(N)}$ is represented as a product of $\tilde{T}_L$, W, and $\tilde{T}_R$, the numerical multiplication $\boldsymbol{x}''' = \tilde{T}^{(N)}\boldsymbol{x}$ can be done very rapidly via the following three steps (Chap. 2(I))

$$x'(\xi' s'_M s_M s_{M+1}\zeta) = \sum_{\xi} \tilde{T}_L(\xi' s'_M|\xi s_M) x(\xi s_M s_{M+1}\zeta)\,, \tag{22}$$

$$x''(\xi' s'_M s'_{M+1} s_{M+1}\zeta) = \sum_{s_M} W(s'_M s'_{M+1}|s_M s_{M+1}) x'(\xi' s'_M s_M s_{M+1}\zeta)\,,$$

$$x'''(\xi' s'_M s'_{M+1}\zeta') = \sum_{s_{M+1}\,\zeta} \tilde{T}_R(s'_{M+1}\zeta'|s_{M+1}\zeta) x''(\xi' s'_M s'_{M+1} s_{M+1}\zeta)\,.$$

One does not have to prepare the $4m^2$-dimensional transfer matrix $\tilde{T}^{(N)}$, containing $16m^4$ matrix elements, explicitly. The Lanczos diagonalization can be accelerated further by an appropriate choice of the initial vector [44–46].

5 Variational State in DMRG

At this point, it is possible to understand the variational nature of the classical (and also quantum) DMRG. Suppose that we have $\tilde{T}^{(N)}$ and the

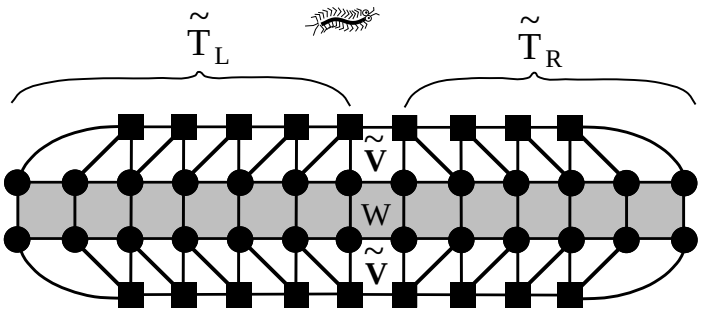

Fig. 5. Graphical representation of the variational eigenvalue of the transfer matrix $T^{(N)}$, see (23). The shaded region represents $T^{(N)}$. The upper and lower parts correspond to the variational state $v^{(N)}$ in (24).

corresponding eigenvector $\tilde{v}^{(N)}(\xi s_M s_{M+1}\zeta)$ from the infinite system algorithm, where $\langle\tilde{v}^{(N)}|\tilde{v}^{(N)}\rangle = 1$ is satisfied. If we form the expectation value $\tilde{\lambda} = \langle\tilde{v}^{(N)}|\tilde{T}^{(N)}|\tilde{v}^{(N)}\rangle$, this can be represented as shown in Fig. 5; the squares denote ξ, ξ', ζ, and ζ' variables which are defined in the renormalization steps. The left and the right halves of the diagram correspond to $\tilde{T}_L(\xi' s'_M|\xi s_M)$ and $\tilde{T}_R(s'_{M+1}\zeta'|s_{M+1}\zeta)$, respectively. As indicated by the filling, all the spin variables are all summed. If we recall that $\tilde{T}_L$ and $\tilde{T}_R$ are created through the iterative use of (21), it is possible to write

$$\langle\tilde{v}^{(N)}|\tilde{T}^{(N)}|\tilde{v}^{(N)}\rangle \;=\; \langle v^{(N)}|T^{(N)}|v^{(N)}\rangle\,, \tag{23}$$

where $v^{(N)}(s_{1\ldots}s_N)$ is the variational state for $T^{(N)}$ defined as

$$\sum_{\{\xi\}\{\zeta\}} \prod_{i=2}^{M-1} A(\xi_{i-1}s_i|\xi_i)\; \tilde{v}^{(N)}(\xi_{M-1}s_M s_{M+1}\zeta_{M+2}) \prod_{j=M+2}^{N-1} B(s_j\zeta_{j+1}|\zeta_j)\,, \tag{24}$$

where $\xi_1 \equiv s_1$ and $\zeta_N \equiv s_N$. This corresponds to the portions in Fig. 5 above and below the original (= unrenormalized) transfer matrix, respectively. We have put the indices to ξ and ζ in order to distinguish the block spin variables. The matrices $A(\xi_{i-1}s_i|\xi_i)$ and $B(s_j\zeta_{j+1}|\zeta_j)$ depend on their position i and j, respectively. Note that $v^{(N)}(s_{1\ldots}s_N)$ is normalized because of the assumed normalization $\langle\tilde{v}^{(N)}|\tilde{v}^{(N)}\rangle = 1$ and the orthogonal relations

$$\begin{aligned}
\sum_{\xi_{i-1}s_i} A(\xi_{i-1}s_i|\xi_i)\, A(\xi_{i-1}s_i|\xi'_i) \;&=\; \delta_{\xi_i\,\xi'_i} \\
\sum_{s_j\zeta_{j+1}}^{m} B(s_j\zeta_{j+1}|\zeta_j) B(s_j\zeta_{j+1}|\zeta'_j) \;&=\; \delta_{\zeta_j\,\zeta'_j}\,.
\end{aligned} \tag{25}$$

Since $T^{(N)}$ is symmetric and positive definite, the largest eigenvalue $\tilde{\lambda}$ of $\tilde{T}^{(N)}$ is a variational lower bound for the largest eigenvalue λ of $T^{(N)}$

$$\tilde{\lambda} = \langle v^{(N)} | T^{(N)} | v^{(N)} \rangle \leq \lambda, \tag{26}$$

and the difference $\epsilon = \lambda - \tilde{\lambda}$ is a decreasing function of m.

It is possible to decompose $\tilde{v}^{(N)}(\xi_{M-1} s_M s_{M+1} \zeta_{M+2})$ further into a matrix product [27], and to write down the variational state in the form

$$v^{(N)}(s_{1\cdots} s_N) \\ = \sum_{\{\xi\}\{\zeta\}} \prod_{i=2}^{M} A(\xi_{i-1} s_i | \xi_i)\ \Omega(\xi_M | \zeta_{M+1}) \prod_{j=M+1}^{N-1} B(s_j \zeta_{j+1} | \zeta_j)\,, \tag{27}$$

where $\Omega(\xi_M | \zeta_{M+1})$ is a $2m$-dimensional diagonal matrix

$$\Omega(\xi_M | \zeta_{M+1}) \;=\; \delta_{\xi_M \zeta_{M+1}} \frac{\omega_{\xi_M}}{\sqrt{\tilde{Z}}}\,. \tag{28}$$

We have imposed the normalization $\Omega^2 = 1$. (Strictly speaking, Ω need not to be diagonal, but $\Omega\Omega^T$ should be.) In the thermodynamic limit $N \to \infty$, the matrices $A(\xi_{i-1} s_i | \xi_i)$ and $B(s_j \zeta_{j+1} | \zeta_j)$ lose the position dependence, and the variational state in (27) coincides with Östlund's matrix-product state (See Chap. 3(I)).

As a result of the infinite-system algorithm, we obtain the variational free energy per site

$$\tilde{f} \;=\; -\frac{1}{N} k_{\mathrm{B}} T \, \log \tilde{\lambda} \tag{29}$$

and other thermodynamic quantities via the numerical derivative of $\tilde{f}$. Since we have the variational state $v^{(N)}(s_{1\cdots} s_N)$ explicitly ((24) and (27)), we can calculate arbitrary spin correlation functions, such as $\langle s_i \rangle = \langle v^{(N)} | \hat{s}_i | v^{(N)} \rangle$ and $\langle s_i s_j \rangle = \langle v^{(N)} | \hat{s}_i \hat{s}_j | v^{(N)} \rangle$, etc. Generally speaking, the numerical precision of $\langle s_i s_j \rangle$ decreases as $|i - j|$ increases.

When we calculate spin correlation functions, we have to check that the energy scale ϵ_m introduced by the restriction of the degrees of freedom is sufficiently small compared with the excitation gap ϵ_g (of $H^{(N)} \equiv -\log \tilde{T}^{(N)} / \Delta$). If not, we have to increase m to keep the numerical precision. If the system is just at the critical temperature $T = T_{\mathrm{c}}$, the gap ϵ_g is of the order of $1/N$. For this reason, it is not reliable to apply the infinite-system algorithm to a classical system just at T_{c}, and directly analyze the thermodynamic limit $N \to \infty$. It would be better to use the finite-system algorithm, that improves the variational state obtained by the infinite-system algorithm further (see Sect.7).

Let us see how accurate the infinite-system algorithm is. Figure 6 shows the specific heat $\mathrm{C_v}(T)$ of the square-lattice Ising model, which is obtained by

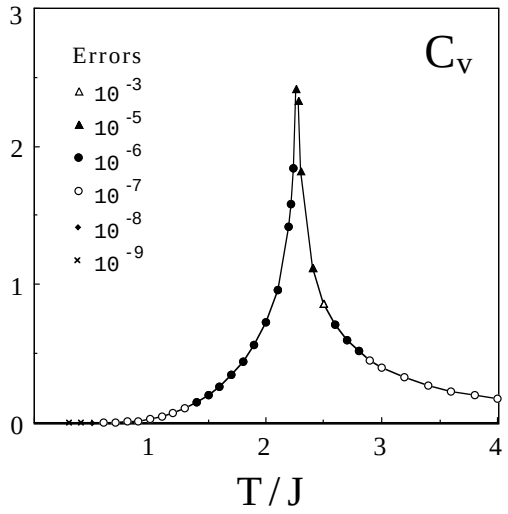

Fig. 6. Calculated specific heat of the Ising model [5].

taking the temperature derivative of the nearest neighbor correlation function $E(T) = \langle s_M s_{M+1} \rangle$. We calculate $E(T)$ for the system up to $N = 2M = 2048$, which is sufficiently larger than the correlation length for each plotted temperature, except at $T = T_c$. The m-dependence for $E(T)$ is negligible when we keep $m = 60$ states. Since we know the exact solution for this model [28], we can directly observe the numerical error in $C_v(T)$; in Fig.6, it is indicated by several marks. The numerical error is not negligible near the critical temperature T_c, partly because $E(T)$ is singular at T_c, and because the numerical derivative

$$\frac{E(T + \Delta T/2) - E(T - \Delta T/2)}{\Delta T} \tag{30}$$

is sensitive to ΔT; typically, we have chosen $\Delta T = 10^{-4}$. The other source of numerical errors is the increase of the cut-off energy scale ϵ_m near T_c, that spoils the numerical precision of the block-spin transformation.

6 History of the Matrix-Product State

Variational states written in the form of matrix products, such as $v^{(N)}$ in (24), have been used for a long time. In this section we review briefly the history of the matrix-product state. In 1941 Kramers and Wannier (K-W) [29,30]

investigated the square lattice Ising model, assuming that the variatonal state can be written as

$$v(\ldots, s_{i-1}, s_i, s_{i+1}, s_{i+2}, \ldots) = \ldots F(s_{i-1}|s_i)F(s_i|s_{i+1})F(s_{i+1}|s_{i+2})\ldots, \quad (31)$$

where $F(s'|s)$ is a 2-dimensional symmetric matrix. The transition temperature $T_{\rm c}$ and the specific heat calculated from this variational state are more accurate than those obtained by the molecular-field and the Bethe approximations [31]. It should be noted that the Gutzwiller approximation [32] for the Hubbard Model [33,34] is quite similar to the K-W approximation.

Around 1960-70 Baxter improved the K-W approximation by introducing additional freedom [18,35]. His variational state is written as

$$v(\ldots, s_{i-1}, s_i, s_{i+1}, s_{i+2}, \ldots) = \sum_{\ldots,a,b,c,d,\ldots} \ldots F_{ab}(s_{i-1}|s_i)F_{bc}(s_i|s_{i+1})F_{cd}(s_{i+1}|s_{i+2})\ldots, \quad (32)$$

where $\ldots a$, b, c, $d\ldots$, denote the additional m-state variables. Since $F_{ab}(s'|s)$ contains $4m^2$ adjustable parameters, the way of finding out the best $F_{ab}(s'|s)$ is non trivial. He performed the optimization using a self-consistent equation for the corner transfer matrix (CTM) [18].

Applications of the matrix-product formulation to quantum systems began with the investigations of Haldane's conjecture. In 1985 Nightingale and Blöte [36] used the K-W matrix product (31) as the initial vector of their projector Monte Carlo simulation. It is interesting that they commented on Baxter's method as follows "... *This method was formulated by Baxter for classical models in statistical mechanics. The generalization to quantum mechanical system is straightforward.*" (The RVA formulation by Martín-Delgado and Sierra can be seen as a realization of this concept; see Chap. 4(I).) In 1987 Affleck, Lieb, Kennedy, and Tasaki [37] showed that the ground state of a special $S = 1$ spin chain can be exactly expressed as

$$\sum_{\ldots,a,b,c,d,e,\ldots} \ldots M_{ab}(s_{i-1})M_{bc}(s_i)M_{cd}(s_{i+1})M_{de}(s_{i+2})\ldots, \quad (33)$$

where $\ldots, a, b, c, d, e, \ldots$ are 2-state variables. They also showed that ground states of this kind exist also for a two-dimensional $S = 3/2$ quantum spin system. Fannes *et al.* generalized the above wave function (33) by assigning m degrees of freedom to $\ldots, a, b, c, d, e, \ldots$. Their variational state is known as 'finitely correlated state,' since the correlation length is always finite [38,39]. Although (33) does not look like (32), they are essentially the same; they are related via a duality transformation. Such a product state has been considered independently in the field of classical diffusion models [40–43].

The variational states in (31)-(33) are uniform. The advantage of the variational state in DMRG ((24) and (27)) is that it allows for a position dependence of the matrices. Because of this, it is possible to treat finite-size systems in the framework of DMRG.

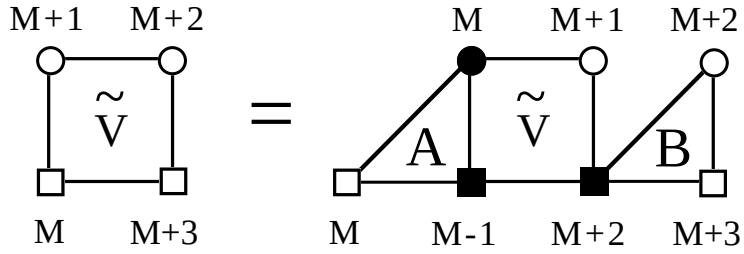

Fig. 7. Position shift of the renormalized state vector $\tilde{v}^{(N)}$ according to (35)-(36).

7 Finite-System Algorithm

The variational state $v^{(N)}(s_{1\ldots}s_N)$ in (24) obtained by the infinite-system algorithm is a good approximation for the eigenvector of $T^{(N)}$, however, it is not the best one. The finite-system algorithm improves the state, so that $\langle v^{(N)}|T^{(N)}|v^{(N)}\rangle$ is maximized under the constraint $\langle v^{(N)}|v^{(N)}\rangle = 1$, keeping at most m states for each block variable.

The algorithm gradually improves the whole variational state

$$\sum_{\{\xi\}\{\zeta\}} \prod_{i=2}^{M-1} A(\xi_{i-1}s_i|\xi_i)\ \tilde{v}^{(N)}(\xi_{M-1}s_M s_{M+1}\zeta_{M+2}) \prod_{j=M+2}^{N-1} B(s_j\zeta_{j+1}|\zeta_j)\,. \quad (34)$$

by directly improving the vector $\tilde{v}^{(N)}$, and indirectly improving other parts by shifting the position of $\tilde{v}^{(N)}$. Assuming that we have already obtained all the matrices shown in (34), we explain the following numerical procedures of the finite system algorithm of the classical DMRG; the main point is the position shift for $\tilde{v}^{(N)}$ [44,45]. Let us create the DSM

$$\tilde{\rho}_L(\xi'_{M-1}s'_M|\xi_{M-1}s_M) = \sum_{s_{M+1}\zeta_{M+2}} \tilde{v}^{(N)}(\xi'_{M-1}s'_M s_{M+1}\zeta_{M+2})\,\tilde{v}^{(N)}(\xi_{M-1}s_M s_{M+1}\zeta_{M+2})\,, \quad (35)$$

and obtain $A(\xi_{M-1}s_M|\xi_M)$ by diagonalizing it. Then, by shifting the position of $\tilde{v}^{(N)}$ as shown in Fig.7

$$\tilde{v}^{(N)}(\xi_M s_{M+1}s_{M+2}\zeta_{M+3}) = \quad (36)$$
$$\sum_{s'_M\xi'_{M-1}\zeta'_{M+2}} \tilde{A}(\xi'_{M-1}s'_M|\xi_M)\tilde{v}^{(N)}(\xi'_{M-1}s'_M s_{M+1}\zeta'_{M+2})\tilde{B}(s_{M+2}\zeta_{M+3}|\zeta'_{M+2})\,,$$

we can construct the new variational state

$$v^{(N)}_{\rm new}(s_{1\ldots}s_N) = \quad (37)$$
$$\sum_{\{\xi\}\{\zeta\}} \prod_{i=2}^{M} A(\xi_{i-1}s_i|\xi_i)\ \tilde{v}^{(N)}(\xi_M s_{M+1}s_{M+2}\zeta_{M+3}) \prod_{j=M+3}^{N-1} B(s_j\zeta_{j+1}|\zeta_j)\,.$$

Compare (37) with (34), the position of $\tilde{v}^{(N)}$ is shifted by one.

The finite-system algorithm can be viewed as maximizing $\langle v_{\rm new}^{(N)}|T^{(N)}|v_{\rm new}^{(N)}\rangle$ via the tuning of $\tilde{v}^{(N)}(\xi_M s_{M+1}s_{M+2}\zeta_{M+3})$, under the constraint $\langle v_{\rm new}^{(N)}|v_{\rm new}^{(N)}\rangle = 1$. This maximization is equivalent to the diagonalization of the (shifted) renormalized transfer matrix

$$\tilde{T}^{(N)}(\xi'_M s'_{M+1}s'_{M+2}\zeta'_{M+3}|\xi_M s_{M+1}s_{M+2}\zeta_{M+3}) = \tilde{T}_L(\xi'_M s'_{M+1}|\xi_M s_{M+1})W(s'_{M+1}s'_{M+2}|s_{M+1}s_{M+2}) \tilde{T}_R(s'_{M+2}\zeta'_{M+3}|s_{M+2}\zeta_{M+3}) \quad (38)$$

to obtain its eigenvector $\tilde{v}^{(N)}(\xi_M s_{M+1}s_{M+2}\zeta_{M+3})$, where we already have $\tilde{T}_R(s'_{M+2}\zeta'_{M+3}|s_{M+2}\zeta_{M+3})$. The half-row transfer matrix $\tilde{T}_L(\xi'_M s'_{M+1}|\xi_M s_{M+1})$ can be easily obtained as

$$\sum_{\xi'_{M-1}s'_M\xi_{M-1}s_M} A(\xi'_{M-1}s'_M|\xi'_M)\tilde{T}_L(\xi'_{M-1}s'_M|\xi_{M-1}s_M) W(s'_M s'_{M+1}|s_M s_{M+1})A(\xi_{M-1}s_M|\xi_M) \quad (39)$$

Thus, by choosing $\tilde{v}^{(N)}$ in (36) as the initial vector of the Lanczos diagonalization for $\tilde{T}^{(N)}$ in (38) [44], one can rapidly improve $\tilde{v}^{(N)}(\xi_M s_{M+1}s_{M+2}\zeta_{M+3})$.

In such a way the finite-system algorithm shifts the position of $\tilde{v}^{(N)}$ to an arbitrary place and improves the variational state site by site [47]. The numerical procedures are basically the same as those in the quantum DMRG explained in Chap. 2(I). It is interesting that such a local improvement (or update) is also used in the zero-temperature QMC simulation for fermionic systems [48].

The advantage of the finite-system algorithm, compared to the infinite one, is its high numerical precision in the calculated thermodynamic quantities and spin correlation functions. The precision is high enough to determine the critical exponents and minor corrections to the scaling hypothesis of a classical system with the help of finite-size scaling [49,50]. Examples are shown in Chaps. 3.2(II) and 3.3(II) by Carlon and Drzewinski [6–8].

8 Corner Transfer Matrix Formulation

We have treated the 2D Ising model on a cylinder, and applied the RG transformation to the row transfer matrix $T^{(N)}$. Remember that the block spin transformation is obtained from the diagonalization of the DSM, which corresponds to a cut in the cylinder (Fig.3). The pictorial image of the DSM suggests that we can define a DSM for any system with arbitrary geometry, just by creating a cut in it. Baxter considered such a construction of the DSM more than 30 years ago [18,35]. He took a square cluster, and expressed the DSM of the system as the fourth power of the so called corner transfer matrix (CTM).

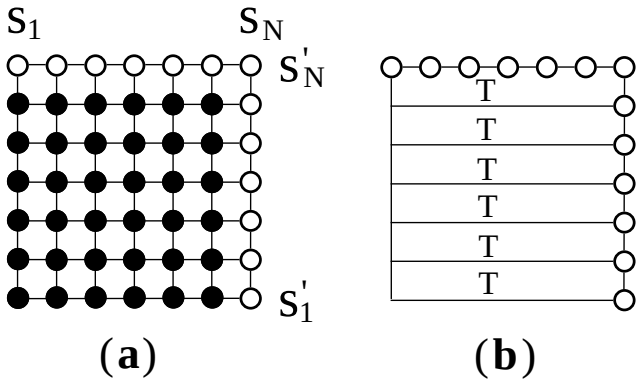

Fig. 8. Construction of the corner transfer matrix $C^{(N)}$, see (40). (**a**) The configuration sum is taken over the spins shown in black. (**b**) It is possible to regard $C^{(N)}$ as a stack of N copies of $T^{(N)}$ with appropriate boundary conditions.

The CTM represents the Boltzmann weight of a square system. Figure 8 (a) shows the corner transfer matrix of the Ising model

$$C^{(N)}(\boldsymbol{s}'|\boldsymbol{s}) = \sum_{\{s\}} \prod_{\langle ijkl\rangle} W(s_i s_j | s_k s_l)\,, \tag{40}$$

where $\langle ijkl\rangle$ represents the neighboring spins around a plaquette W, and the sum is taken over all the spins shown in black. By definition, $C^{(N)}(\boldsymbol{s}'|\boldsymbol{s})$ is block diagonal, because s'_N in $\boldsymbol{s}' = s'_{1\ldots}s'_N$ and s_N in $\boldsymbol{s} = s_{1\ldots}s_N$ are the same; in other words, $C^{(N)}(\boldsymbol{s}'|\boldsymbol{s})$ for $s'_N \neq s_N$ is always zero. It is also possible to construct $C^{(N)}$ by stacking N transfer matrices: $N \times T^{(N)}$. (See Fig. 8 (b).) The system is then enlarged by joining another row and column to the square. This is done by multiplying horizontal and vertical transfer matrices T and a plaquette W as shown in Fig. 9 (a). Formally this means $C^{(N)}(\boldsymbol{s}'|\boldsymbol{s}) \to C^{(N+1)}(\boldsymbol{s}'_{\rm new}|\boldsymbol{s}_{\rm new}) = C^{(N+1)}(s'_{1\ldots}s'_{N+1}|s_{1\ldots}s_{N+1})$ with

$$C^{(N+1)}(\boldsymbol{s}'_{\rm new}|\boldsymbol{s}_{\rm new}) = \sum_{\boldsymbol{s}'''\boldsymbol{s}''} \delta_{s'_{N+1}s_{N+1}} W(s_N s_{N+1}|s''_N s'_N) \tag{41}$$
$$T^{(N)}(\boldsymbol{s}'|\boldsymbol{s}''')T^{(N)}(\boldsymbol{s}|\boldsymbol{s}'')C^{(N)}(\boldsymbol{s}'''|\boldsymbol{s}'')\,.$$

At the same time we extend the length of $T^{(N)}$ by joining a plaquette W as shown in Fig. 9 (b) in order to prepare for the next extension $C^{(N+1)} \to C^{(N+2)}$. The extension $T^{(N)} \to T^{(N+1)}$ is essentially the same as (21).

Baxter constructed the DSM as the fourth power of the CTM

$$\rho_{\rm c}(\boldsymbol{s}''''|\boldsymbol{s}) = \sum_{\boldsymbol{s}'''\boldsymbol{s}''\boldsymbol{s}'} C^{(N)}(\boldsymbol{s}''''|\boldsymbol{s}''')C^{(N)}(\boldsymbol{s}'''|\boldsymbol{s}'')C^{(N)}(\boldsymbol{s}''|\boldsymbol{s}')C^{(N)}(\boldsymbol{s}'|\boldsymbol{s})\,. \tag{42}$$

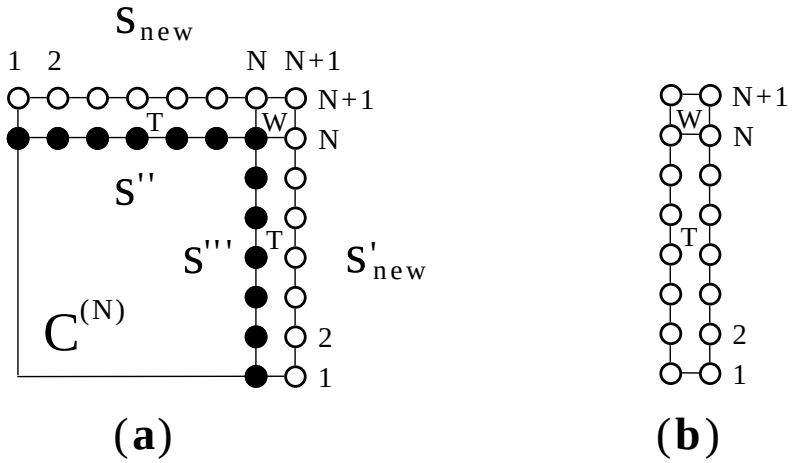

Fig. 9. Enlargement of the CTM: (a) $C^{(N+1)}$ is obtained by joining two $T^{(N)}$ and a W to $C^{(N)}$, see (41). (b) The extension $T^{(N)} \to T^{(N+1)}$, see (21).

This is not far from the conventional definition of DSM in DMRG (8), because ρ_{c} can be written as

$$\rho_{\mathrm{c}}(\boldsymbol{s}'_L|\boldsymbol{s}_L) = \sum_{\boldsymbol{s}_R} v(\boldsymbol{s}'_L|\boldsymbol{s}_R) v(\boldsymbol{s}_L|\boldsymbol{s}_R)\,, \tag{43}$$

where the vector $v(\boldsymbol{s}_L|\boldsymbol{s}_R)$ is given by

$$v(\boldsymbol{s}_L|\boldsymbol{s}_R) = \sum_{\boldsymbol{s}} C^{(N)}(\boldsymbol{s}_L|\boldsymbol{s}) C^{(N)}(\boldsymbol{s}|\boldsymbol{s}_R)\,. \tag{44}$$

Note that $v(\boldsymbol{s}_L|\boldsymbol{s}_R)$ is block diagonal, as $C^{(N)}(\boldsymbol{s}'|\boldsymbol{s})$ is. Figure 10 shows the graphical representation of ρ_{c}, that corresponds to a $2N-1$ by $2N-1$ square with a cut, where the cut extends from an edge to the center. Thus $Z^{(2N-1)} = \mathrm{Tr}\,\rho_{\mathrm{c}}$ is the partition function of the $2N-1$ by $2N-1$ square system.

Using the CTM, Baxter calculated the variational free energy (per site) of 2D lattice models in the limit $N \to \infty$ by solving a self-consistent equation. Okunishi pointed out that Baxter's method is basically the same as the infinite-system algorithm of the classical DMRG [51]. Compared to the classical DMRG, Baxter's method has the advantage that the numerical calculation is very fast, since it does not require diagonalizations of large scale matrices. Nishino and Okunishi introduced this advantage into the DMRG and formulated a numerical RG algorithm, which is called 'corner-transfer-matrix renormalization group' (CTMRG) [52,53].

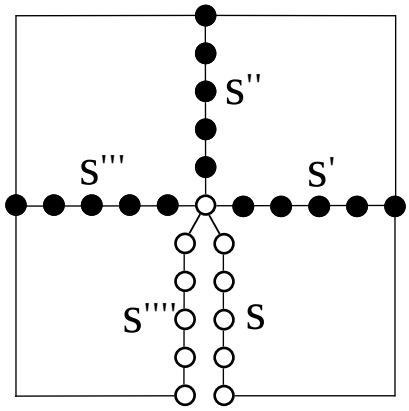

Fig. 10. Baxter's construction of the DSM as the fourth power of a CTM (42).

The outline of the CTMRG is as follows. The diagonalization of the DSM

$$\rho_{\rm c}(\boldsymbol{s}'|\boldsymbol{s}) \;=\; \sum_{\xi} A(\boldsymbol{s}'|\xi)\,\alpha_\xi^4\,A(\boldsymbol{s}|\xi) \tag{45}$$

defines the RG transformation $\boldsymbol{s} \to \xi$ via the orthogonal matrix $A(\boldsymbol{s}|\xi)$. For example, $C^{(N)}$ can be renormalized as

$$\tilde{C}^{(N)}(\xi'|\xi) \;=\; \sum_{\boldsymbol{s}'\boldsymbol{s}} A(\boldsymbol{s}'|\xi')C^{(N)}(\boldsymbol{s}'|\boldsymbol{s})A(\boldsymbol{s}|\xi) \;=\; \delta_{\xi'\xi}\,\alpha_\xi\,, \tag{46}$$

where ξ' and ξ are m-state block variables. One thing one has to keep in mind is that $\rho_{\rm c}$ is block diagonal, as $C^{(N)}$ is, and therefore the block variable ξ implicitly includes the spin variable s_N, the central spin in Fig. 10. The variational partition function of the $2N-1$ by $2N-1$ square is then expressed as

$$\tilde{Z}^{(2N-1)} = \mathrm{Tr}\,\tilde{\rho}_{\rm c} = \mathrm{Tr}\,\left(\tilde{C}_{\rm c}^{(N)}\right)^4 = \sum_{\xi=1}^{m}\alpha_\xi^4\,. \tag{47}$$

As the infinite-system algorithm, the CTMRG consists of the successive mappings $\tilde{C}^{(N)} \to \tilde{C}^{(N+1)} \to \tilde{C}^{(N+2)}$ using the enlargement of the system (41) and the RG transformation (46). As a result, we obtain $\tilde{Z}^{(2N-1)} \to \tilde{Z}^{(2N+1)} \to \tilde{Z}^{(2N+3)} \to \cdots$ up to arbitrary system sizes, starting from a small N ($N = 2$ or 3).

Numerical data calculated by the CTMRG can be used for a finite-size scaling analysis of classical systems. Figure 11 shows the N-dependence of the local order parameter $\langle s\rangle$ of the Ising model at the center of a $(2N-1)$ by $(2N-1)$ square, when $T = T_{\rm c}$. Fixed boundary conditions (all spins up at the boundary) are chosen. We plot representative data for both $m = 4$

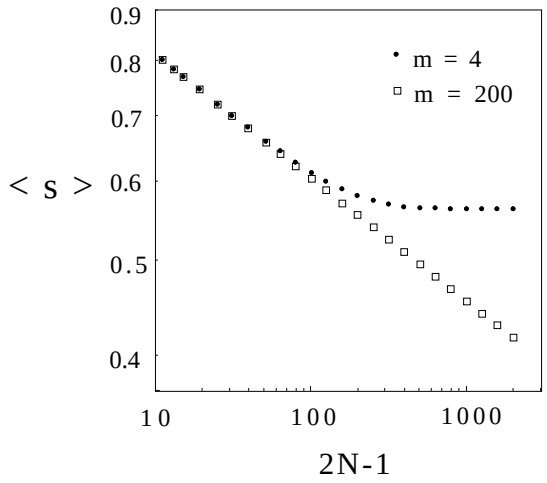

Fig. 11. Order parameter of the Ising model at the center of a $(2N-1)$ by $(2N-1)$ square when $T = T_c$.

and $m = 200$ up to $2N - 1 = 19999$. At criticality, the local order parameter obeys the scaling formula

$$\langle s \rangle \propto (2N-1)^{-(d-2+\eta)/2}\,, \tag{48}$$

where d is the spatial dimension ($d = 2$). Indeed, the calculated parameter $\langle s \rangle$ is almost proportional to $(2N-1)^{-1/8}$. The least-square fitting to the data in the range $199 \leq 2N-1 \leq 19999$ gives $\eta = 0.2501$, which is quite close to the exact one $\eta = 1/4$. In the same manner, we can determine another exponent ν from the nearest neighbor spin correlation $E_{2N-1} = \langle s's \rangle$ at the center of the $(2N-1)$ by $(2N-1)$ system, that obeys the scaling form

$$E_{2N-1} - E_\infty \propto (2N-1)^{1/\nu - d}\,. \tag{49}$$

From the calculated data for $199 \leq 2N-1 \leq 19999$, we obtain $\nu = 1.0006$. Again, the numerical result agrees with the exact exponent $\nu = 1$.

The CTMRG is also useful to detect a latent heat L. As an example, let us calculate L of the $q = 5$ Potts model [54], which shows a weak first order transition. (It was impossible to determine L by Monte Carlo simulations because L is quite small.) Figure 12 shows the calculated local energy at the center of a $(2N-1)$ by $(2N-1)$ square system for both fixed (= ordered) and free (= disordered) boundary conditions, up to $2N-1 \leq 3999$ for $m = 40, 67$ and 200. Though there is a non-negligible m-dependence, it is clear that the model does not show a second order transition. A double extrapolation with respect to N and m gives the latent heat $L = 0.027$ which agrees with the exact result $L \sim 0.0265$ [18,20]. This is the first quantitative numerical estimate of L for the $q = 5$ Potts model.

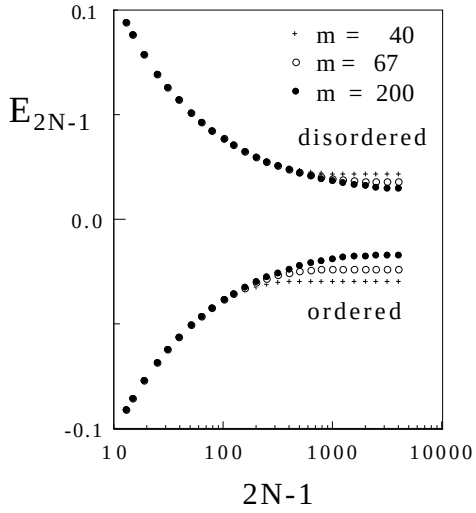

Fig. 12. Local energy E_{2N-1} of the $q = 5$ Potts model at the center of a $(2N-1)$ by $(2N-1)$ square, calculated for the ordered and the disordered phase. The zero of the energy has been shifted to the average of the two quantities [18,20].

Finally we mention that Baxter's construction of the DSM can be generalized to any dimension [55–57]. For example, consider a cubic cluster of a 3D Ising model, and divide it into 8 subcubes. As a direct extension of the CTM in 2D, we can imagine 'corner tensors' $C^{(N)}(a|b|c)$ that correspond to the Boltzmann weight for a subcube; the tensor indices $a = \left(a_{ij}\right)$, $b = \left(b_{ij}\right)$, and $c = \left(c_{ij}\right)$ represent 2D spin arrays on the surfaces of the subcubes. Figure 13 shows the pictorial image of the DSM $\rho_{\rm cube}(a|b)$, which is constructed as a contraction between 8 corner tensors. In 3D, the DSM corresponds to a cut in the cube. We obtain the RG transformation from the surfaces a, b, and c to m-state block spins by diagonalizing $\rho_{\rm cube}(a|b)$. The enlargement of the corner cube can be performed via a 3D generalization of Fig.9. Thus, as far as the formulation is concerned, we can extend CTMRG to 3D systems.

More generally, by breaking up a n-dimensional *hypercube* into 2^n-numbers of *hyper-corner-cubes*, we can define a DSM for a $(n-1)$-dimensional surface of the hyper-corner cube. Once we have obtained the DSM, we can define the block-spin transformation, and can apply RG transformations to the hypercubic system. Since the renormalized *hyper-corner tensor* has m^n numbers of elements, numerical calculations in higher dimension are much more difficult than in 2D. [58]

9 Discussion

We finally list several unsolved problems in classical DMRG.

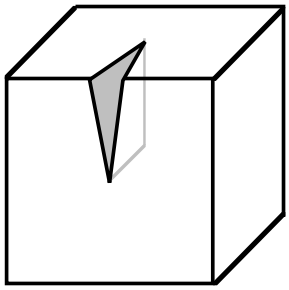

Fig. 13. The density matrix for a 3D cube, constructed from eight corner tensors. This is a generalization of Fig.9.

- The matrix-product variational state for a finite-size system with periodic boundary conditions (= finite-size ring) should be translational invariant, however, the finite-system algorithm does not give such a translational invariant state [59].
- The way to apply classical DMRG to models with long-range interaction is not known; it is even difficult to define a transfer matrix for such models.
- It is not straightforward to treat random classical systems, because the transfer-matrix eigenvalue can be negative, and because the RG transformation depends on the position of block spins [60].
- To treat systems with continuous site variables or systems defined in continuous space (-time), we have to first discretize them [61]; we do not know the general principle for such a discretization that is suitable for DMRG.

We hope that these problems will be solved in the near future. [62]

The authors thank the organizers of the DMRG '98 workshop at the Max-Planck-Institut für Physik komplexer Systeme in Dresden. T. N. thanks I. Peschel, E. Carlon, G. Sierra, M. A. Martín-Delgado, X. Wang and T. Xiang for the discussions on classical DMRG. Numerical calculations were done using NEC SX-4 in the computer center of Osaka University. Y. H. is partly supported by the Sasakawa Scientific Research Grant from The Japan Science Society. K. O. and T. H. are partially supported by a Grant-in-Aid from the Ministry of Education, Science and Culture of Japan.

References

1. S. R. White, Phys. Rev. Lett. **69**, 2863 (1992); Phys. Rev. **B48**, 10345 (1993)
2. H. F. Trotter, Proc. Am. Math. Soc. **10**, 545 (1959)
3. M. Suzuki, Prog. Theor. Phys. **56**, 1454 (1976)
4. R. P. Feynmann and A. R. Hibbs, Quantum Mechanics and Path Integrals, McGraw-Hill, (1965)
5. T. Nishino, J. Phys. Soc. Jpn. **64**, 3598 (1995)
6. E. Carlon and A. Drzewiński, Phys. Rev. Lett. **79**, (1997) 1591; Phys. Rev. **E57**, 2626 (1998)
7. E. Carlon and F. Igloi, Phys. Rev. **B57**, 7877 (1998); F. Igloi and E. Carlon, cond-mat/9805083
8. E. Carlon, A. Drzewiński and J. Rogiers, Phys. Rev. **B58**, 5070 (1998)
9. R. J. Bursill, T. Xiang, G. A. Gehring, J. Phys. Condensed Matter L583-L590 (1996)
10. X. Wang and T. Xiang, Phys. Rev. **B56**, 5061 (1997)
11. F. Naef, X. Wang, X. Zotos, and W. van der Linden, cond-mat/9812117
12. N. Shibata, J. Phys. Soc. Jpn **66**, 2221 (1997)
13. B. Ammon, M. Troyer, T.M. Rice, and N. Shibata, cond-mat/9812144
14. Y. Honda and T. Horiguchi, Phys. Rev. **E56**, 3920 (1997)
15. S. Östlund and S. Rommer, Phys. Rev. Lett **75**, 3537 (1995); S. Rommer and S. Östlund, Phys. Rev. **B55**, 2164 (1997); M. Andersson, M. Boman, and S. Östlund, cond-mat/9810093
16. It is possible to fix the boundary spins to consider more general boundary conditions.
17. There is a bibliography of Ising in cond-mat/9605174.
18. R. J. Baxter, Exactly Solved Models in Statistical Mechanics, Academic Press, London, (1982)
19. R. B. Potts, Proc. Camb. Phil. Soc.**48**, 106
20. F. Y. Wu, Rev. Mod. Phys. **54**, 235 (1982), and references therein.
21. Baxter used another definition of the density submatrix in his variational method [18], where his density submatrix is block diagonal, see (42)-(44).
22. T. Nishino and K. Okunishi, in Strongly Correlated Magnetic and Superconducting Systems, Eds. G. Sierra and M. A. Martín-Delgado, Springer Berlin, (1997)
23. Eigenvalues of the DSM can be negative when the system contains randomness.
24. I. Peschel, M. Kaulke and Ö. Legeza, cond-mat/9810174
25. Strictly speaking, the density matrix eigenvalues do not decay exponentially; See K. Okunishi, Y. Hieida, and Y. Akutsu, cond-mat/9810239
26. C. Lanczos: J. Res. Nat. Bur. Std. **45**, 255 (1950)
27. The Numerical recipes home page (`http://cfata2.harvard.edu/numerical-recipes/`) is useful to know about numerical linear algebra. Also it is worth reading J. Wilkinson, The Algebraic Eigenvalue Problem, Oxford, London, (1965)
28. L. Onsager, Phys. Rev. **65**, 117 (1944)
29. H. A. Kramers and G. H. Wannier, Phys. Rev. **60**, 263 (1941)
30. R. Kikuchi, Phys. Rev. **81**, 988 (1951)
31. H. A. Bethe, Proc. Roy. Soc. **A150**, 552 (1935)
32. M. C. Gutzwiller, Phys. Rev. **137**, A1726 (1965)

33. J. Kanamori, J. Phys. Soc. Jpn. **30**, 275 (1963)
34. J. Hubbard, Proc. Roy. Soc. **A276**, 238 (1963); **A281**, 401 (1964)
35. R. J. Baxter, J. Math. Phys. **9**, 650 (1968); R. J. Baxter, J. Stat. Phys. **19**, 461 (1978)
36. N. P. Nightingale and H. W. Blöte: Phys. Rev. **B33**, 659 (1986)
37. I. Affleck, T. Kennedy, E. H. Lieb and H. Tasaki, Phys. Rev. Lett. **59**, 799 (1987)
38. M. Fannes, B. Nachtergale and R. F. Werner, Europhys. Lett. **10**, 633 (1989); M. Fannes, B. Nachtergale and R. F. Werner, Commun. Math. Phys. **144**, 443 (1992); M. Fannes, B. Nachtergale and R. F. Werner, Commun. Math. Phys. **174**, 477 (1995)
39. A. Klümper, A. Schadschneider and J. Zittarz, Z. Phys. **B87**, 281 (1992); H. Niggemann, A. Klümper and J. Zittartz, Z. Phys. **B104**, 103 (1997)
40. B. Derrida and M. R. Evans, J. Phys. A: Math. Gen. **26**, 1493 (1993)
41. N. Rajewsky, L. Santen, A. Schadschneider, M. Schreckenberg, cond-mat/9710316
42. A. Honecker, I. Peschel, J. Stat. Phys. **88**, 319 (1997)
43. Y. Hieida, J. Phys. Soc. Jpn. **67**, 369 (1998)
44. S. R. White, Phys. Rev. Lett. **77**, 3633 (1996)
45. T. Nishino and K. Okunishi, J. Phys. Soc. Jpn. **64**, 4084 (1995)
46. U. Schollwöck, Phys. Rev. **B58**, 8194 (1998)
47. A modification of the whole variational state is more time consuming. The situation is similar to the 'Order N' problem in the density functional formalism.
48. S. R. White, D. J. Scalapino, R. L. Sugar, E. Y. Loh, J. E. Gubernatis and R. T. Scalettar, Phys. Rev. **B40**, 506 (1989)
49. M. E. Fisher, in Proc. Int. School of Physics 'Enrico Fermi', Ed. M.S. Green, Academic Press, New York, (1971), Vol. **51**, p. 1.
50. M. N. Barber, in Phase Transitions and Critical Phenomena, Ed. C. Domb and J. L. Lebowitz, Academic Press, New York, (1983), Vol. **8**, p. 146. and references therein.
51. K. Okunishi, Thesis, Osaka University 1996 (in Japanese); Thesis, Osaka University 1999 (in English). (Contact to `okunishi@godzilla.phys.sci.osaka-u.ac.jp`)
52. T. Nishino and K. Okunishi, J. Phys. Soc. Jpn. **65**, 891 (1996); T. Nishino and K. Okunishi, J. Phys. Soc. Jpn. **66**, 3040 (1997)
53. T. Nishino, K. Okunishi, and M. Kikuchi, Physics Letters **A213**, 69 (1996)
54. T. Nishino and K. Okunishi, J. Phys. Soc. Jpn. **67**, 1492 (1998)
55. T. Nishino and K. Okunishi, J. Phys. Soc. Jpn. **67**, 3066 (1998)
56. G. Sierra and M. A. Martín-Delgado, cond-mat/9811170.
57. Y. Hieida, K. Okunishi, and Y. Akutsu, cond-mat/9901155.
58. A way to decrease the computational effort in higher dimension is to perform RG transformations *before* creating the new RG transformations; it is possible, because the (infinite-system) DMRG is a self consistent method. [1,45]
59. The numerical precision in DMRG for a system with periodic boundary conditions is lower than that for a system with open boundary conditions. The reason can be understood by looking at the variational state written as a matrix product.
60. Position dependence *in the quantum Hamiltonian* can be treated by quantum DMRG; K. Hida, J. Phys. Soc. Jpn. **65**, 895 (1996)

61. S. G. Chung, J. Phys.: Cond. Matt. **9**, L619 (1997); Current Topics in Physics, Ed. Y. M. Cho, J. B. Hong, and C. N. Yang, vol. **1**, World Scientific, Hongkong, p.295 (1998)
62. The authors will list up the latest information about DMRG in this URL: `http://quattro.phys.sci.kobe-u.ac.jp/dmrg.html`